LANGMUIR

pubs.acs.org/Langmuir Article

Modulating the Influenza A Virus–Target Membrane Fusion Interface With Synthetic DNA–Lipid Receptors

Elizabeth R. Webster,[‖] Katherine N. Liu,[‖] Robert J. Rawle, and Steven G. Boxer*

Cite This: *Langmuir* 2022, 38, 2354–2362 Read Online

ACCESS | Metrics & More | Article Recommendations | Supporting Information

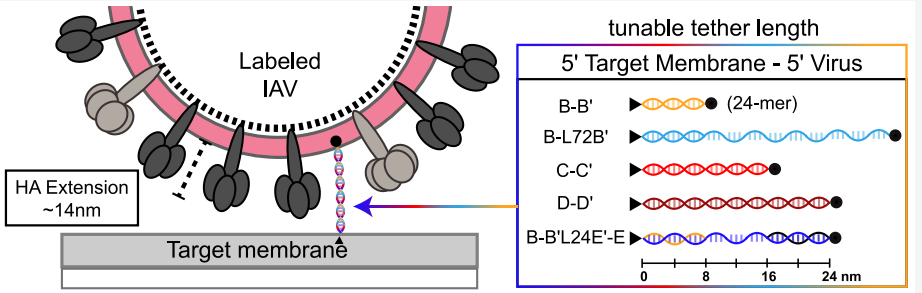

ABSTRACT: Influenza A virus (IAV) binds to sialylated glycans on the cell membrane before endocytosis and fusion. Cell-surface glycans are highly heterogeneous in length and glycosylation density, which leads to variations in the distance and rigidity with which IAV is held away from the cell membrane. To gain mechanistic insight into how receptor length and rigidity impact the mechanism of IAV entry, we employed synthetic DNA–lipids as highly tunable surrogate receptors. We tethered IAV to target membranes with a panel of DNA–lipids to investigate the effects of the distance and tether flexibility between virions and target membranes on the kinetics of IAV binding and fusion. Tether length and the presence of a flexible linker led to higher rates of IAV binding, while the efficiencies of lipid and content mixing were typically lower for longer and more rigid DNA tethers. For all DNA tether modifications, we found that the rates of IAV lipid and content mixing were unchanged. These results suggest that variations in the interface between IAV and a target membrane do not significantly impact the rate-limiting step of fusion or the low-pH-triggered engagement of viral fusion peptides with the target membrane. However, our results imply that the flexibility of the viral receptor is important for ensuring that hemifusion events are able to successfully proceed to pore formation.

INTRODUCTION

Before viral infection can occur, enveloped viruses must undergo viral membrane fusion, where the viral envelope mixes with a target membrane, and the viral genome is transferred into a target cell. The process of bringing two membranes together to form a hemifusion intermediate, or lipid mixing, is thermodynamically favored but has a high kinetic barrier.[1,2] To overcome this barrier, viral fusion proteins undergo a large conformational change and insert a hydrophobic peptide or loop into the host membrane and then the proteins collapse to bring the viral and host membranes together.[3,4] For this process to successfully occur, the viral fusion peptide and the target membrane must be in close physical proximity.

Proteins expressed on the host cell membrane surface act as viral receptors and provide sustained interaction between the virus and host membrane. For some viruses like Ebola, human immunodeficiency virus (HIV), and SARS-CoV-2, the viral (co-)receptor is extremely specific and can mechanistically play a role in facilitating viral entry.[5−8] For other viruses like influenza A virus (IAV), the cell-surface receptor that IAV binds to is not responsible for initiating fusion, so IAV can bind to a variety of targets on the cell surface. IAV binds to the outside of a cell through an interaction of its fusion protein, hemagglutinin (HA), with sialic acid moieties, which are displayed on many different cell-surface glycans.[9,10] At neutral pH, HA extends roughly 13.5 nm from the IAV envelope.[10] Due to the promiscuity of glycan sialylation, HA can bind to a wide array of glycolipids and glycoproteins that display α2-3 and α2-6 linkages of sialic acid, which leads to variations in the distance between a bound virion and the cell membrane.[11,12]

After IAV binding and endocytosis, low pH triggers HA to undergo a large conformational rearrangement, where its hydrophobic fusion peptide (HAfp) relocates by 10 nm to insert into the host membrane.[13] Kinetic simulations and single-virus studies have found that at least three neighboring HAfps must successfully engage with the target membrane to initiate a fusion event.[14,15] However, because most single-virus

Received: December 5, 2021
Revised: January 26, 2022
Published: February 10, 2022

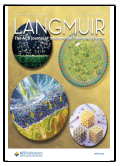

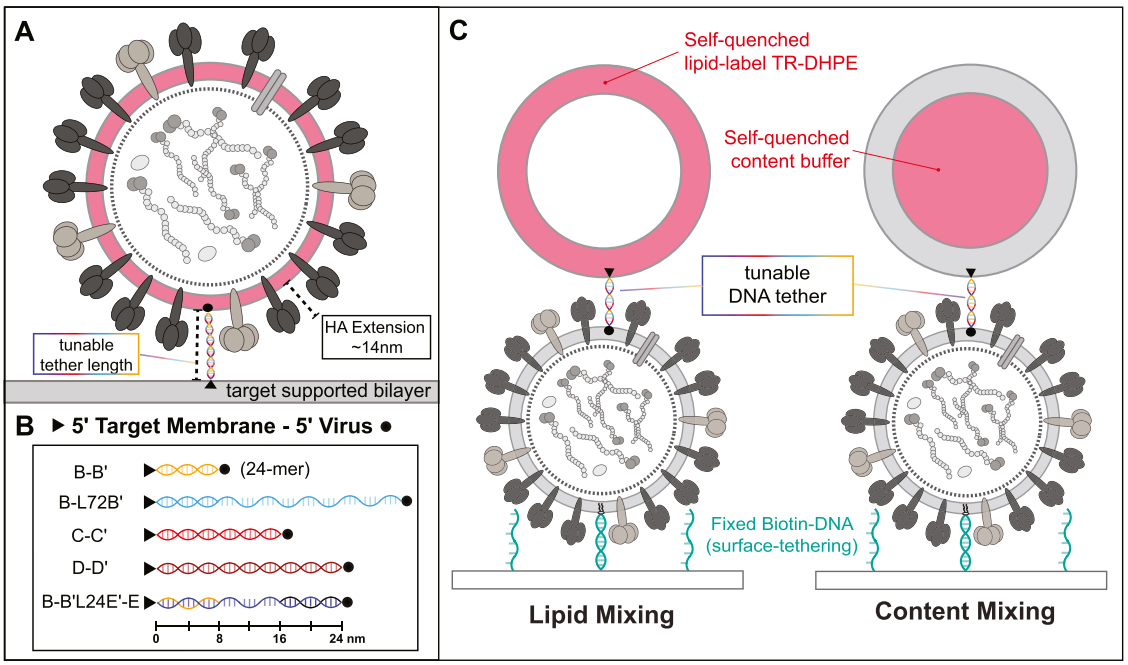

Figure 1. Schematic of IAV−membrane binding and fusion assays with the DNA tethers employed in this study. (A) Single-virus binding assay: A DNA−lipid displayed on the IAV envelope (red) hybridizes with the complementary sequence displayed on a supported lipid bilayer (gray). (B) Schematic representation of the DNA tethers used in lipid and content mixing experiments (for full DNA−lipid and DNA oligo sequences, see Table S1). One end of each DNA tether is target membrane anchored (triangle) and the other is anchored in the IAV envelope (circle). (C) Single-virus lipid mixing assays: Glass surfaces are functionalized with biotinylated-DNA through PLL-*g*-PEG biotin/neutrAvidin interaction. Influenza virions contain two orthogonal sequences of DNA−lipids (green, rainbow). Fixed DNA sequences (green) are used for surface-tethering virions. Tunable DNA−lipids (rainbow) hybridize with either lipid-labeled vesicles (left, red) or content-labeled vesicles (right, red) to form DNA tethers of various lengths and rigidities. A single DNA−lipid tether is shown for clarity.

fusion measurements utilize homogenous sialylated lipids as viral receptors, there are still unanswered questions about how variations in the distance and rigidity of the IAV−target membrane interface affect the mechanism of IAV fusion.

We have previously employed DNA−lipids (Figure S1) as tunable synthetic receptors for both viral and vesicle fusion. DNA−lipids can spontaneously insert into viral and model membranes under aqueous conditions, and complementary sequences can be easily designed to tether two membranes at a controlled distance through DNA hybridization.[16,17] DNA−lipids have been successfully utilized as surrogate receptors to monitor single-virus binding and fusion events.[17,18] When IAV is bound through DNA tethers to target vesicles of various membrane compositions, in particular varying the mol fraction of cholesterol, the kinetics of IAV lipid mixing are indistinguishable from when IAV is bound to the sialic acid of the ganglioside GD1a, regardless of the number of DNA tethers.[17,18] These results implied that cholesterol-mediated clustering of sialic acid viral receptors displayed on the target membrane has no effect on IAV fusion kinetics;[19] however, there was no exploration of how DNA tether sequence and length affect the viral fusion process.

The effect of DNA tether sequence and orientation has been explored in both ensemble and single-vesicle measurements of vesicle fusion, where synthetic surrogates were utilized as SNARE mimics.[20−23] We found that adding a flexible linker to the membrane-proximal ends of a DNA tether increased the rate of vesicle tethering and docking, while the kinetics of vesicle fusion were only minimally impacted by sequence length and identity.[20,21] We hypothesize that similar changes to the DNA tether sequences used to facilitate IAV fusion could also affect the processes of IAV binding and virus membrane fusion.

Here, we create and implement a panel of DNA−lipids with varying lengths and rigidities as surrogate viral receptors (Figure 1). We use these DNA tethers to modulate the interface between IAV and a target membrane to study how tether length, flexible linker length, and tether rigidity affect the single-virus kinetics of IAV binding, lipid mixing, and content mixing. This strategy yields insights into the crucial role of receptor flexibility in facilitating IAV−membrane fusion.

MATERIALS AND METHODS

Materials. Palmitoyl oleoyl phosphatidylcholine (POPC), dioleoyl phosphatidylethanolamine (DOPE), and cholesterol (CH) were purchased from Avanti Polar Lipids (Alabaster, AL). Texas Red-1,2-dihexadecanoyl-*sn*-glycero-3-phosphoethanolamine (TR-DHPE), Oregon Green-1,2-dihexadecanoyl-*sn*-glycero-3-phosphoethanolamine (OG-DHPE), fatty acid depleted bovine serum albumin (BSA), and neutrAvidin were purchased from ThermoFisher Scientific (Waltham, MA). Sepharose CL-4B and disialoganglioside GD1a from bovine brain (Cer-Glc-Gal(NeuAc)-GalNAc-Gal-NeuAc) were purchased from Sigma-Aldrich (St. Louis, MO). Organic solvents and buffer salts were obtained from Fisher Scientific (Pittsburgh, PA) and Sigma-Aldrich (St. Louis, MO). Polydimethylsiloxane (PDMS) was obtained from Ellsworth Adhesives (Hayward, CA). Poly(L-lysine)-graft-poly(ethylene glycol) (PLL-*g*-PEG) and Poly(L-lysine)-*graft*-poly-(ethylene glycol) biotin (PLL-*g*-PEG biotin) were purchased from SuSoS AG (Dübendorf, Switzerland). Influenza A virus (strain X-31, A/Aichi/68, H3N2) is a BSL-2 agent that was obtained from Charles River Laboratories (Wilmington, MA). IAV was handled following an approved administrative biosafety panel protocol at Stanford University. No other unexpected or unusually high safety hazards were encountered with this work.

https://doi.org/10.1021/acs.langmuir.1c03247
Langmuir 2022, 38, 2354−2362

Buffers. The following buffers were used. HB buffer: 20 mM HEPES, 150 mM NaCl, pH 7.2. Vesicle buffer: 10 mM NaH_2PO_4, 90 mM sodium citrate, 150 mM NaCl, pH 7.4. For lipid and content mixing experiments, fusion buffer: 10 mM NaH_2PO_4, 90 mM sodium citrate, 150 mM NaCl, pH 5.1. SRB content buffer: 30 mM sulforhodamine B (SRB), 10 mM NaH_2PO_4, 90 mM sodium citrate, 120 mM NaCl, pH 7.4.

Microscopy and Analysis. All epifluorescence micrographs and videos were acquired with a Nikon Ti-U microscope using a 100× oil immersion objective, NA = 1.49 (Nikon Instruments, Melville, NY), a Spectra-X LED Light Engine (Lumencor, Beaverton, OR) as an excitation light source, and an Andor iXon 897 EMCCD camera (Andor Technologies, Belfast, U.K.) with 16-bit image settings. Images were captured with Metamorph software (Molecular Devices, Sunnyvale, CA). Images were analyzed with FIJI and adapted versions of previously published MATLAB scripts.[17,24]

Additional Microscopy Information. Additional excitation/emission filter wheels were used: Texas Red filter cube (ex = 562/40 nm, bs = 593 nm, em = 624/40 nm) excitation (ex = 560/55 nm) and emission (em = 645/75 nm); NBD filter cube (ex = 475/35 nm, bs = 509 nm, em = 528/38 nm) (ex = 460/50 nm) and emission (em = 535/50 nm).

DNA−Lipid Synthesis. DNA−lipids (structure shown in Figure S1) were synthesized using phosphoramidite coupling, as previously described.[20] Critically, the membrane anchor is a saturated dialkyl glyceryl ether with octadecyl groups, which allows the DNA−lipids to insert spontaneously into a membrane under aqueous conditions. DNA−lipids do not partition out of the membrane as it has been shown for single cholesterol anchored groups.[25,26] Specific DNA−lipids used in this work are described in Table 1 and full sequences are listed in Table S1. Biotinylated-DNA was synthesized by the PAN facility at Stanford University and diluted to the desired concentration in deionized (DI) water. All DNA oligos were stored at −20 °C.

Table 1. Description of DNA−Lipids Used in This Study[a]

sequence name	total number of bases	description
A	24	nonspecific hybridization
A′	24	nonspecific hybridization
B	24	specific overlap
B′	24	specific overlap
L24B′	48	linker + specific overlap
L42B′	66	linker + specific overlap
L72B′	96	linker + specific overlap
C	48	specific overlap
C′	48	specific overlap
D	72	specific overlap
D′	72	specific overlap
E	24	specific overlap
B′L24E′	72	specific + linker + specific

[a]All single-stranded DNA sequences have a lipid at the 5′ end, except for B′L24E′, which is a DNA oligo with no membrane anchor. See Table S1 for full sequences. Sequences that start with the same letter (ex. A/A′) indicate sense−antisense complementarity. The letter L denotes a flexible polyT or polyC linker followed by the number of nt in the linker. Nonspecific refers to polyA/polyT complementarity, whereas specific oligos have nonrepeating sequences, which must overlap completely with the complementary sequence for binding to occur.

Viral Preparation and DNA−Lipid Incorporation. For binding experiments, influenza was labeled with TR-DHPE; DNA−lipids were incorporated into the viral envelope, as previously described.[17] Briefly, a solution of IAV (0.4 mg/mL viral protein concentration) and TR-DHPE was gently rocked at room temperature for 2 h before pelleting by centrifugation at 21 130 rcf for 50 min and resuspending in HB buffer to yield a ∼0.2 mg/mL viral protein concentration solution. The solution was stored on ice and used or aliquoted and frozen within 3 days. For lipid and content mixing experiments, unlabeled IAV was pelleted in HB buffer by centrifugation at 21 130 rcf for 50 min and resuspended in fresh HB buffer for a final viral protein concentration of 2 mg/mL. For all experiments, DNA−lipids were incubated with the final virus suspension on ice overnight.

Vesicle Preparation and DNA−Lipid Incorporation. Large unilamellar vesicles (LUVs) containing DNA−lipids were created following established protocols.[21] Briefly, lipid mixtures were prepared in chloroform, gently dried under a stream of argon gas, and the film was further dried under house vacuum for at least 3 h. Dried lipid films were resuspended in vesicle buffer or SRB content buffer by vortexing at a lipid concentration of 0.56 mM, extruded at least 30 times (15 passes on each side) through a 100 nm pore size membrane, and stored at 4 °C until use. All vesicle solutions were used within 3 days of extrusion. For binding experiments, DNA−lipids were added to the vesicles at 0.01 mol % of the total lipid concentration. For lipid and content mixing experiments, DNA−lipids were added at 0.05 mol % of the total lipid concentration. For all experiments, DNA−lipids were incorporated into vesicles overnight at 4 °C. Content-labeled vesicles were purified from free SRB content buffer on a CL-4B size-exclusion column immediately before use in a content mixing experiment. After equilibration, content-labeled vesicles were used within four hours.

Single-Virus Binding Assay. Virus binding assays were performed using supported lipid bilayers (SLBs) and TR-DHPE labeled IAV (see Figure 1A). SLBs displaying DNA were created following established protocols.[27] Briefly, LUVs (nominally 50 or 100 nm in diameter, 69.9 POPC: 20 DOPE: 10 CH: 0.1 OG-DHPE) containing a DNA−lipid sequence were added to a PDMS microfluidic flow cell, incubated for roughly 15 min, and rinsed with deionized water (DI) and vesicle buffer to form a uniform SLB. This SLB was imaged to ensure that it was defect free before adding TR-DHPE labeled IAV. IAV was allowed to bind with the SLB through DNA hybridization, extensively rinsed, and imaged using fluorescence microscopy. The resulting number of bound virions per microscope field of view (FOV) was quantified through spot analysis of fluorescence micrographs using custom MATLAB scripts.

Lipid and Content Mixing Assays. The single lipid and content mixing architectures were prepared, as shown in Figure 1 as previously described.[18] In a microfluidic flow cell (see the Supporting Information for details), glass slides displaying DNA sequence A were functionalized, as previously described.[18] Next, 5 μL of IAV in HB buffer (roughly 5.4 nM) displaying sequences A′ (antisense to A) and a sequence of interest (Tables 1 and S1) were introduced to the flow cell and tethered to the substrate. After rinsing the flow cell with vesicle buffer, the surface was further passivated by incubating 10 μL of bovine serum albumin (BSA, 1 mg/mL) for at least 10 min to prevent nonspecific binding of added target vesicles. Finally, 2−3 μL of ∼100 nm diameter vesicles (40 POPC: 20 DOPE: 40 CH) displaying DNA−lipids and containing content buffer were introduced (2.8 μM nominal total lipid concentration). Lipid- or content-labeled vesicles were allowed to bind for 5−10 min to control surface density and ensure spatial separation between particles. Excess unbound vesicles and BSA were removed by rinsing the flow cell with vesicle buffer.

Fluorescence microscopy was used to collect image streams of 1200 frames at a frame rate of 3.47 frames/s (Movies S1 andS2). After the image stream was started, the pH of the flow cell was rapidly exchanged from 7.4 to 5.1 using fusion buffer. The exchange time was calibrated using OG-DHPE vesicles in a separate experiment, as done previously.[17] The time between introduction of low pH to the FOV and dequenching events was then analyzed using custom MATLAB scripts.[17,24]

RESULTS AND DISCUSSION

We synthesized a panel of DNA−lipids (Table 1) to test the effects of tether length, the presence of a flexible linker, and tether rigidity on the kinetics of IAV fusion. For the remainder of this manuscript, we use the terms "DNA oligo" or "DNA−

https://doi.org/10.1021/acs.langmuir.1c03247
Langmuir 2022, 38, 2354−2362

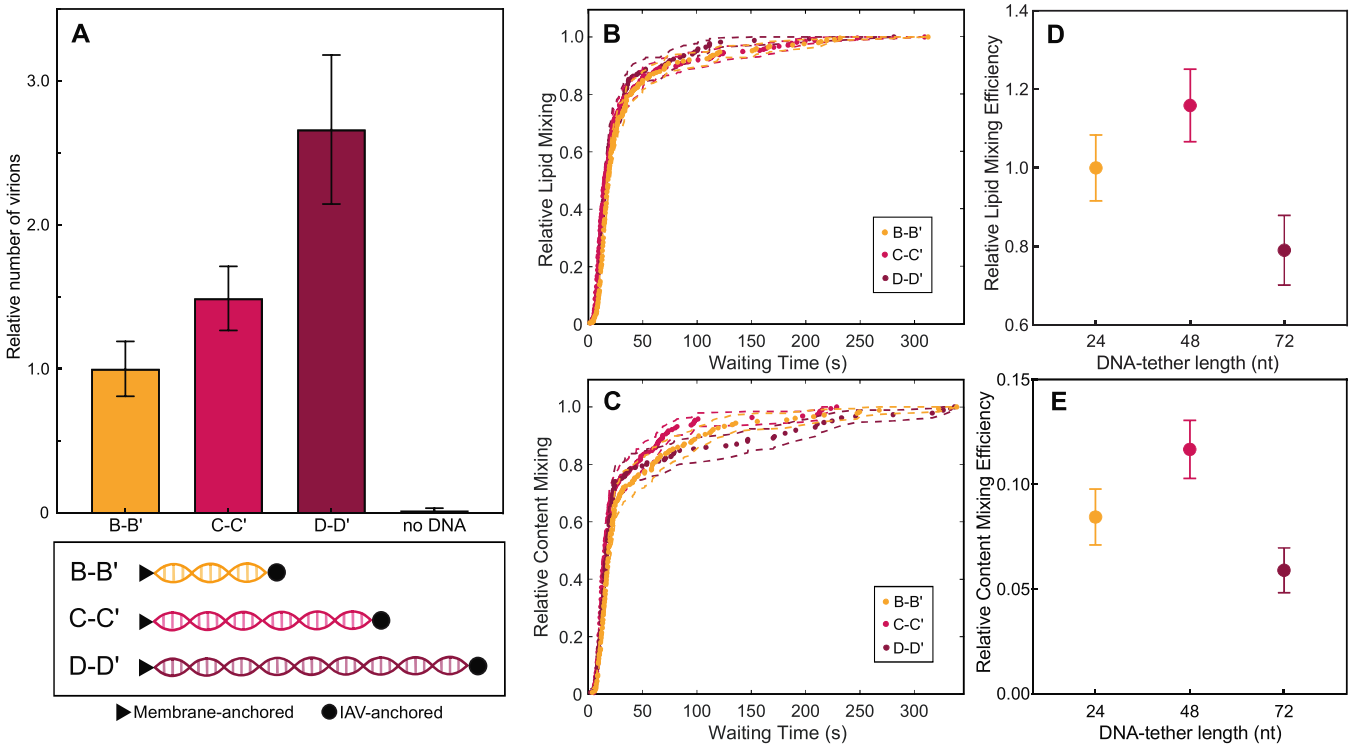

Figure 2. Contrasting effects of DNA tether length on IAV binding and fusion kinetics. The DNA sequences that comprise each tether are listed in pairs (membrane anchored−IAV anchored). (A) Tether length increases the number of IAV that bind to an SLB (assay geometry shown in Figure 1A). Values represent the relative number of virions bound per microscope FOV ± standard deviation within sample replicates, where the value for B−B′ is normalized to 1. (B) Tether length has no effect on the rates of lipid mixing or (C) content mixing (fusion assay geometry shown in Figure 1C). Wait times from pH drop to content mixing for individual fusion events were plotted as cumulative distribution functions (CDFs). For all DNA tether lengths, the rates of IAV lipid and content mixing are the same within bootstrap resampling error (95% confidence intervals). (D) Relative efficiencies of lipid mixing and (E) content mixing decrease when IAV is tethered to a target membrane with a 72-nt fully overlapping DNA tether in comparison to 24 and 48-nt tethers. Lipid and content mixing efficiencies are normalized to the lipid mixing value for the 24-nt tether to allow for direct comparison, and points represent the average efficiency value ± bootstrap resampling error. Individual CDFs and absolute efficiencies are reported in Figure S3.

lipid" to describe a single DNA sequence, while the term "DNA tether" refers to 2−3 complementary DNA oligos or DNA−lipids that bind through DNA hybridization at the membrane−IAV interface. For simplicity, complementary sequences are named using the same letter, (ex. A/A′), which indicates sense−antisense complementarity (see Table S1 for full sequences). Some DNA−lipids, DNA oligos, and DNA tethers contain single-stranded, flexible regions. These regions are referred to as "linkers" and are comprised of polyT or polyC sequences. The number of nucleotides (nt) in a linker is indicated in the sequence name with the letter L followed by the number of nt (ex. L24 indicates a 24-nt linker).

DNA−lipids were incorporated into the IAV envelope by incubating virions with an aqueous suspension of DNA−lipids. When sequence E (Table S1) was incubated with IAV at the concentrations used in this study, there was a median of 7 DNA−lipids incorporated per virion.[18] All DNA−lipids contained the same lipidic anchor, and as a result, we expected the extent of DNA−lipid incorporation into the IAV envelope to be consistent across all DNA sequences, regardless of sequence identity. For each sequence, the concentration of DNA−lipids was carefully calibrated by UV absorbance before addition to IAV or target vesicles to ensure that binding differences were attributable to the DNA sequence and not to differences in DNA concentration.

We utilized a single-virus binding assay (Figure 1A) to quantify the relative availability of various DNA−lipid sequences that were anchored in the IAV envelope and to ensure that viral binding was sequence-specific. We created SLBs that each displayed one of the DNA sequences in a microfluidic flow cell. Next, we introduced TR-DHPE labeled IAV that displayed the complementary DNA sequence to the flow cell. Virions were allowed to bind to the SLB through DNA hybridization for a set time interval, and the resulting number of stably bound virions per microscope field of view (FOV) was quantified through image processing of fluorescence micrographs taken at various positions on the SLB around the microfluidic flow cell.

We then used single-virus fusion assays to characterize the impact of tether length on the kinetics of lipid and content mixing (Figure 1C). Unlabeled virions display two orthogonal sequences of DNA−lipids: one for surface-tethering IAV (seq. A) and one with a variable sequence for tethering IAV to a target vesicle (Tables 1 and S1). Previous work has shown that increasing the number of DNA−lipids added to the IAV envelope does not significantly change the rate of lipid mixing.[17] Once virions were surface-tethered to a passivated glass slide in a microfluidic flow cell through DNA hybridization (A/A′), target vesicles (with a nominal diameter of 100 nm) displaying the complementary DNA sequence were introduced and allowed to bind to IAV. For lipid mixing experiments, vesicles were lipid-labeled with a self-quenched concentration of TR-DHPE. For content mixing experiments, vesicles contained a self-quenched concentration of SRB

https://doi.org/10.1021/acs.langmuir.1c03247
Langmuir 2022, 38, 2354−2362

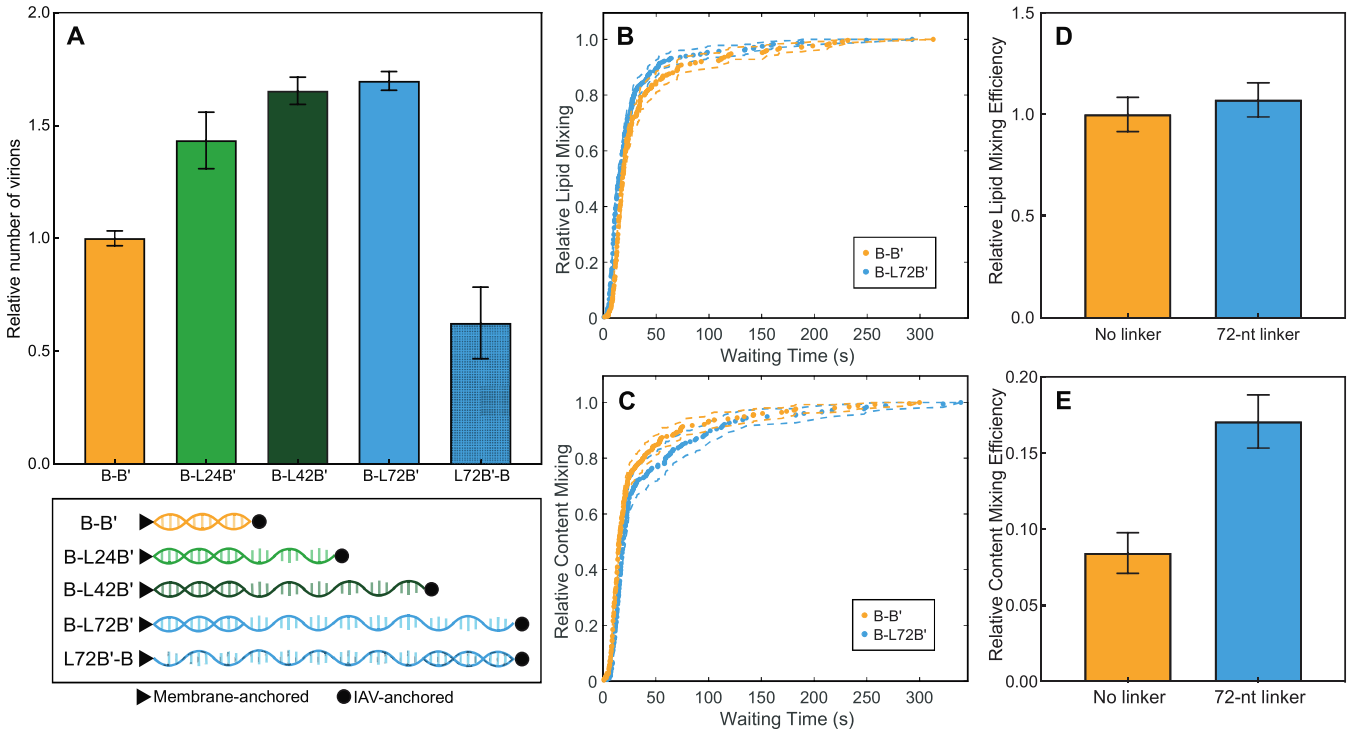

Figure 3. Adding a flexible linker to the IAV-proximal end of a DNA tether increases viral binding and content mixing efficiency but has no effect on the lipid mixing efficiency or the rates of lipid and content mixing. (A) Flexible linker increases the number of IAV that bind to an SLB when the tethered sequence is anchored in the IAV envelope (assay geometry shown in Figure 1A). Values represent the relative number of virions bound per microscope FOV ± standard deviation within sample replicates, where the value for B−B′ is normalized to 1. (B) Presence of a flexible linker has no significant effect on the rates of lipid mixing or (C) content mixing (assay geometry shown in Figure 1C). Wait times from pH drop to content mixing for individual fusion events were plotted as cumulative distribution functions (CDFs). In the presence and absence of a flexible linker, the rates of IAV lipid and content mixing are the same within bootstrap resampling error (95% confidence intervals). (D) Flexible linker has no effect on the efficiency of lipid mixing, while (E) it leads to a two-fold increase in the content mixing efficiency. Both lipid and content mixing values are normalized to the lipid mixing efficiency for the 24-nt tether with no linker, and points represent the average efficiency value ± bootstrap resampling error. Individual CDFs and absolute efficiencies are reported in Figure S4.

content buffer (Figure 1C). For both lipid and content mixing experiments, vesicles, rather than virus, were labeled to avoid the process of adding a large amount of dye to the virion envelope or viral contents. The amount of time that vesicles were allowed to bind was varied for different DNA sequences to ensure a comparable spatial density and a total number of vesicles for each experiment. Finally, the buffer was rapidly exchanged from pH 7.4−5.1 and the fluorescence intensity of lipid- or content-labeled vesicles was monitored through video micrographs. To minimize light exposure, we monitored lipid and content mixing in separate experiments.

Effect of Tether Length. To characterize the role of target membrane proximity in the mechanism of IAV fusion, we synthesized pairs of DNA−lipids that would hybridize to form fully overlapping tethers with 24-nt (B−B′), 48-nt (C−C′), and 72-nt (D−D′, see Table S1 for full sequences). We first compared the availability of IAV-anchored DNA oligos and the rate of IAV binding by using the single-virus binding assay (assay geometry shown in Figure 1A). Nonspecific binding was found to be negligible when IAV was introduced to an SLB that displayed no DNA and no sialic acid. For all sequences, the number of IAV bound was dramatically higher than nonspecific binding. Increasing the length of the DNA tether increases the relative number of virions that bind to an SLB over a standardized time interval.

By contrast, when vesicles are bound instead of a virus, increasing tether length did not lead to a significant change in the number of vesicles that bind to an SLB (Figure S2), which suggests that when DNA lipids are anchored in the IAV envelope, the viral glycoprotein bulk decreases the availability of shorter DNA sequences.

Next, we tethered target vesicles to IAV using the fully overlapping DNA tethers to observe single-virus fusion kinetics (assay geometry shown in Figure 1C). The wait times from pH drop to lipid or content mixing for individual fusion events were extracted and plotted in cumulative distribution functions (CDFs, Figure 2B,C, traces expanded in Figure S3). Surprisingly, increasing the tether length had no effect on either the rates of IAV lipid or content mixing. However, we observed a slight decrease in the efficiencies of lipid and content mixing for the 72-nt tether (Figure 2D,E) in comparison to the 24 and 48-nt tethers. Efficiency is calculated as the number of fusion events observed over the total number of particles analyzed. Relative efficiency is used throughout the text to more easily examine trends observed between different DNA−lipid sequences. Absolute efficiencies of lipid and content mixing are reported in the Supporting Information. While tether length increased binding and decreased fusion efficiencies, all three tether lengths led to the same rates of lipid and content mixing, which implies that increasing tether length up to the distances studied here does not alter the IAV−membrane interface in a manner that changes the rate-limiting step of fusion.

https://doi.org/10.1021/acs.langmuir.1c03247
Langmuir 2022, 38, 2354−2362

It is relevant to compare the tether heights with the distance that HA extends from the IAV membrane at neutral and low pH. In comparison to HA, which extends roughly 13.5 nm from the IAV envelope at neutral pH, the double-helical 24-nt tether is slightly shorter (8 nm), the 48-nt tether is of a comparable height (16 nm), and the 72-nt tether is significantly longer (24 nm).[28] Interestingly, the calculated tether distance for the 72-nt tether is greater than the total extension of HA at low pH, while the 24-nt tether is shorter than the height of HA at neutral pH.

The observation that IAV binding and fusion occur with DNA tethers of lengths 8, 16, and 24 nm suggests that DNA−lipid-mediated binding is not constrained by the height of HA and that the presence of DNA tethers does not limit the ability of viral HA to contact the membrane. The change in fusion efficiencies as a result of tether length suggests that a later step in the fusion process, such as the depth or the orientation of HAfps after the initial process of HA engagement, may be affected by the height and presence of the DNA tethers.

One critical difference between tethering IAV to a target membrane via DNA hybridization as opposed to a sialic acid containing moiety is that the surrogate receptor does not have a direct interaction with HA. Additionally, our experiments take place in buffer conditions at which the DNA hybridization process is essentially irreversible, whereas the HA−sialic acid interaction is reversible and relatively weak (∼mM dissociation constant).[29] These differences may explain why the 24 and 72-nt tethers were still able to stably bind and facilitate IAV fusion; the DNA tethers are mobile within both membranes and can shift away from the site of HA engagement. This is supported by previous variable incidence angle-fluorescence interference contrast (VIA-FLIC) microscopy measurements, which found that DNA tethers of various lengths can spontaneously reorganize to alter the height of the junction between two membranes.[27] While these explanations remain speculative, it is possible that molecular dynamics simulations or electron microscopy could visualize the orientation of DNA lipids during the fusion process to further elucidate this point.

Effect of a Flexible Linker. Next, we sought to study the effect of adding a single-stranded linker of varying lengths to increase the flexibility of the DNA tether. We added a single-stranded DNA linker of 24-nt (L24B′), 42-nt (L42B′), and 72-nt (L72B′) to the 5′ end (next to the lipid anchor) of the B′ sequence. We introduced these DNA−lipids to the IAV envelope and then created SLBs that displayed a DNA sequence that was complementary to the fully overlapping region of the IAV-anchored sequence.

When the linker DNA oligo was incorporated into the IAV envelope, increasing the length of the flexible linker led to an increase in the number of IAVs bound within a given time interval as the linker length was extended from zero to 24−42-nt; however, between 42 and 72-nt, there was a limited increase in binding. When the linker oligo was anchored in the SLB, IAV binding was lower than all other permutations in which the linker was IAV-proximal (Figure 3A).

We then took the longest linker sequence, L72B′, and utilized it in the single-virus fusion assays to understand how the presence of a flexible linker would affect the kinetics of lipid and content mixing. When we plotted the wait times to lipid and content mixing for individual fusion events in CDFs and compared for each DNA tether, the rates of lipid and content mixing were unchanged in the presence of a flexible linker (Figure 3B,C, traces expanded in Figure S4). Both DNA tethers also led to comparable lipid mixing efficiencies (Figure 3D), but the presence of a flexible linker led to a two-fold increase in the content mixing efficiency (Figure 3E).

The overall increase in IAV binding due to the presence of a flexible linker is generally consistent with previous work on DNA-mediated vesicle-vesicle binding.[30] IAV binding only increased when the linker was located at the IAV-proximal end of the DNA tether, whereas binding decreased when the linker was located at the membrane-proximal end of the tether. When vesicles are tethered to an SLB, the addition of a flexible linker on the vesicle-proximal end of the DNA tether does not lead to a significant difference in the extent of binding (Figure S5). As a result, we hypothesize that the flexible linker may allow for the overlapping sequence to extend away from the crowded IAV−membrane surface when it is anchored in the viral envelope while offering no additional flexibility when the linker is anchored in the target membrane.

If we assume that the maximal length of the flexible linker is comparable to a double-stranded DNA helix, then we can crudely approximate that the 42-nt linker could extend up to ∼14 nm, which is similar to the length that HA extends from the IAV envelope at neutral pH.[10] The presence of this linker would enable the overlapping portion of the DNA−lipid to extend beyond HA and increase its availability for hybridization. Consequently, it appears that once the maximal extension of the linker approaches the height of HA, further increasing the linker length does not result in significantly higher levels of IAV binding (Figure 3A).

The addition of a flexible linker on the IAV-proximal end of the DNA tether did not lead to any significant changes in the rates of lipid or content mixing, which indicates that there was no perturbation to the rate-limiting step of lipid mixing, or the timescale of low-pH-triggered engagement of HAfp with the target membrane. However, we did observe that the presence of a 72-nt linker roughly doubled the content mixing efficiency, which suggests that IAVs bound through a rigid tether are less likely to proceed from hemifusion to pore formation.

The decrease in productive pore formation with rigid linkers may be related to HAfp engagement within the target membrane. NMR studies have shown that mutations to the IAV HAfp can affect the depth and angle of HAfp engagement with a target membrane at low pH, which can subsequently eliminate IAV fusion activity.[31,32] It is not fully understood why some mutations lead to a stalled hemifusion intermediate, but it has been observed that WT HAfp adopts a 105° angle within the bilayer, and mutations that adopt shallower angles either result in leaky fusion or no fusion.[33] Our data in conjunction with previous work suggest that the presence of a flexible linker enables the HAfp to more often sample an orientation within the target membrane that allows for the successful progression from hemifusion to pore formation, in comparison to a rigid, fully overlapping tether with no flexible linker.

Rigidity of Tether. Finally, we sought to understand the effect of tether rigidity on the kinetics of IAV fusion. Single-stranded DNAs require significantly less energy to bend relative to double-stranded helices,[34] so we hypothesized that adding a flexible hinge to the middle of a DNA tether would enable the tethers to more easily contract at the IAV−target membrane interface during the process of lipid mixing.

To create a flexible hinge in the middle of a 72-nt tether, we designed three DNAs that would hybridize to form two 24-nt, fully overlapping regions at the IAV and target membrane-

https://doi.org/10.1021/acs.langmuir.1c03247
Langmuir 2022, 38, 2354−2362

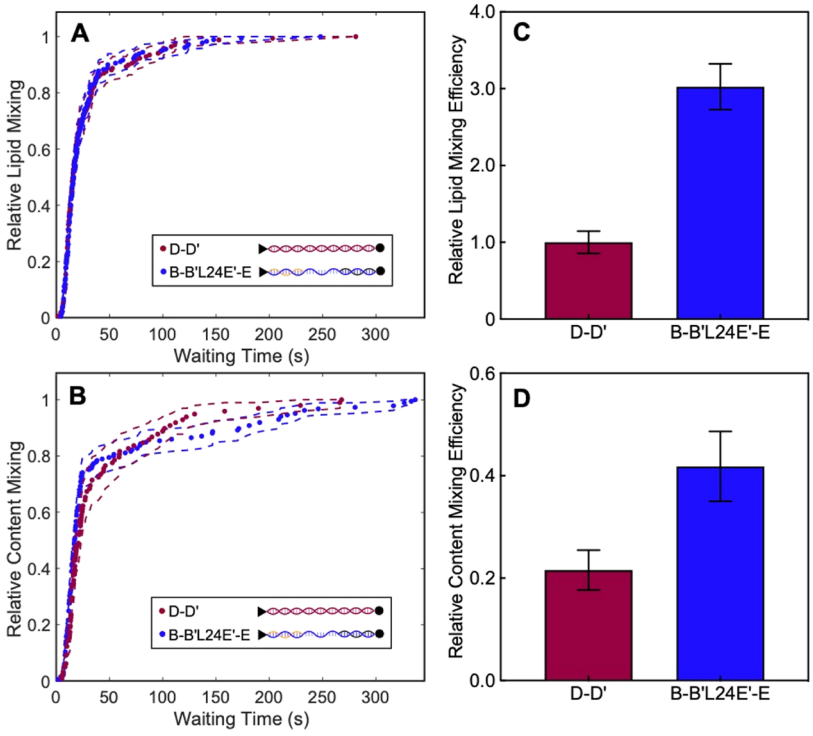

Figure 4. Tether rigidity decreases fusion efficiency but has no effect on the rates of lipid mixing and content mixing. (A) Increasing the flexibility of the middle of the tether has no effect on the rates of lipid mixing or (B) content mixing (assay geometry shown in Figure 1C). Wait times from pH drop to content mixing for individual fusion events were plotted as cumulative distribution functions (CDFs). For both tether rigidities, the rates of IAV lipid and content mixing are the same within bootstrap resampling error (95% confidence intervals). (C) Flexible hinge increased the lipid mixing efficiency by three-fold and (D) increased the content mixing by two-fold. Lipid and content mixing efficiencies are normalized to the lipid mixing efficiency of D−D′, and points represent the average efficiency value ± bootstrap resampling error. Individual CDFs and absolute efficiencies are reported in Figure S7.

proximal ends, while leaving a flexible 24-nt linker in the middle of the tether (B−B′L24E′−E, Figure 1C). We incubated target vesicles with sequence E and a three-fold excess of the DNA oligo with sequence B′L24E′. Excess free DNA was purified away from vesicle solutions on a size-exclusion column. When these vesicles were introduced to an SLB or tethered IAV that displayed sequence B, the vesicles were able to bind through DNA hybridization (Figure S6).

We compared the flexible hinge tether (B−B′L24E′−E) with a fully overlapping, rigid tether (D−D′) of the same total length (72-nt) using the single-virus fusion assays. The wait times from pH drop to lipid or content mixing for individual fusion events for each DNA tether were extracted and plotted in CDFs and compared (Figure S7). Similar to other DNA tether modifications, the existence of a flexible hinge to the middle of the DNA tether did not lead to a significant difference in the rates of lipid mixing (Figure 4A) or content mixing (Figure 4B). However, the efficiency of both fusion processes was enhanced by the presence of the flexible hinge, where lipid mixing efficiency displayed a three-fold increase (Figure 4C) and content mixing efficiency displayed a two-fold increase (Figure 4D).

As in other tether perturbations, the rates of lipid and content mixing were unchanged by tether rigidity. The consistency of fusion rates supports the theory that tether rigidity does not affect the rate-limiting step of fusion or successful insertion of a critical number of neighboring HAfp into the target membrane. In contrast to the IAV-proximal linker, the presence of a flexible hinge increased the efficiencies of both lipid mixing and content mixing, rather than just the efficiency of content mixing. One explanation for the increase in lipid mixing efficiency is that positioning the flexible hinge in the middle of the DNA tether rather than at the IAV-proximal end may enable HAfps to obtain a favorable orientation within the target membrane that increases the fraction of hemifusion and full fusion events.

CONCLUSIONS

We have tethered IAV to target membranes using DNA−lipids of different lengths and rigidities to understand how modulating physical properties of the virus-target membrane interface affects the mechanism of IAV−membrane fusion. We show that altering the membrane−IAV distance and tether rigidity does not impact the rate-limiting step of lipid and content mixing, whereas the efficiencies of lipid and content mixing are sensitive to tether flexibility. These results imply that despite the receptor heterogeneity of cell-surface glycans, HAfps can still productively engage with a target membrane across a large range of distances and that the efficacy of IAV fusion is enhanced by receptor flexibility. This work has implications for how the rigidity and distance between biological interfaces impact other membrane fusion processes and downstream signaling.[35−38] While our DNA tethering methodology yields several mechanistic insights into the role of viral receptor length and flexibility in IAV fusion, direct visualization of the membrane interface would further elucidate the role of tether mobility in the mechanism of IAV fusion.

https://doi.org/10.1021/acs.langmuir.1c03247
Langmuir 2022, 38, 2354−2362

■ ASSOCIATED CONTENT

Supporting Information

The Supporting Information is available free of charge at https://pubs.acs.org/doi/10.1021/acs.langmuir.1c03247.

Supporting Information includes full sequences of the DNA−lipids used in this work, individual cumulative distribution functions and the absolute efficiencies of lipid and content mixing, additional binding data and controls (PDF)

Micrograph of lipid mixing of Texas-Red labeled vesicles bound to surface-tethered influenza A virions (unlabeled) (AVI)

Micrograph of content mixing of SRB content-labeled vesicles bound to surface-tethered influenza A virions (unlabeled) (AVI)

■ AUTHOR INFORMATION

Corresponding Author

Steven G. Boxer − *Department of Chemistry, Stanford University, Stanford, California 94305, United States;* orcid.org/0000-0001-9167-4286; Email: sboxer@stanford.edu

Authors

Elizabeth R. Webster − *Department of Chemistry, Stanford University, Stanford, California 94305, United States;* Present Address: Sandia National Laboratories, Livermore, California 94550, United States; orcid.org/0000-0003-2764-1118

Katherine N. Liu − *Department of Chemistry, Stanford University, Stanford, California 94305, United States;* Present Address: University of Notre Dame, Lucy Family Institute for Data & Society, Notre Dame, Indiana 46556, United States.; orcid.org/0000-0001-9869-5979

Robert J. Rawle − *Department of Chemistry, Stanford University, Stanford, California 94305, United States;* Present Address: Williams College, Department of Chemistry, Williamstown, Massachusetts 01267, United States.; orcid.org/0000-0003-4958-4919

Complete contact information is available at: https://pubs.acs.org/10.1021/acs.langmuir.1c03247

Author Contributions

‖E.R.W. and K.N.L. contributed equally to this work. E.R.W. and K.N.L. designed experiments, performed experiments, analyzed data, and co-wrote the article. R.J.R. and S.G.B. designed experiments and co-wrote the article. All authors have given approval to the final version of the manuscript.

Notes

The authors declare no competing financial interest.

■ ACKNOWLEDGMENTS

E.R.W. was supported by the Center for Molecular Analysis and Design and by a National Science Foundation Graduate Research Fellowship. K.N.L. was supported by a National Science Foundation Graduate Research Fellowship. This work was supported by a National Institutes of Health Grant R35 GM118044 (S.G.B.).

■ REFERENCES

(1) Harrison, S. C. Viral Membrane Fusion. *Virology* **2015**, *479−480*, 498−507.

(2) Chernomordik, L. V.; Kozlov, M. M. Mechanics of Membrane Fusion. *Nat. Struct. Mol. Biol.* **2008**, *15*, 675−683.

(3) Chernomordik, L. V.; Frolov, V. A.; Leikina, E.; Bronk, P.; Zimmerberg, J. The Pathway of Membrane Fusion Catalyzed by Influenza Hemagglutinin: Restriction of Lipids, Hemifusion, and Lipidic Fusion Pore Formation. *J. Cell Biol.* **1998**, *140*, 1369−1382.

(4) White, J. M.; Delos, S. E.; Brecher, M.; Schornberg, K. Structures and Mechanisms of Viral Membrane Fusion Proteins. *Crit. Rev. Biochem. Mol. Biol.* **2008**, *43*, 189−219.

(5) Blumenthal, R.; Durell, S.; Viard, M. HIV Entry and Envelope Glycoprotein-Mediated Fusion. *J. Biol. Chem.* **2012**, *287*, 40841−40849.

(6) Benton, D. J.; Wrobel, A. G.; Xu, P.; Roustan, C.; Martin, S. R.; Rosenthal, P. B.; Skehel, J. J.; Gamblin, S. J. Receptor Binding and Priming of the Spike Protein of SARS-CoV-2 for Membrane Fusion. *Nature* **2020**, *588*, 327−330.

(7) Fénéant, L.; Szymańska-de Wijs, K. M.; Nelson, E. A.; White, J. M. An Exploration of Conditions Proposed to Trigger the Ebola Virus Glycoprotein for Fusion. *PLoS One* **2019**, *14*, No. e0219312.

(8) Costello, D. A.; Millet, J. K.; Hsia, C.-Y.; Whittaker, G. R.; Daniel, S. Single Particle Assay of Coronavirus Membrane Fusion with Proteinaceous Receptor-Embedded Supported Bilayers. *Biomaterials* **2013**, *34*, 7895.

(9) Sauter, N. K.; Hanson, J. E.; Glick, G. D.; Brown, J. H.; Crowther, R. L.; Park, S. J.; Skehel, J. J.; Wiley, D. C. Binding of Influenza Virus Hemagglutinin to Analogs of Its Cell-Surface Receptor, Sialic Acid: Analysis by Proton Nuclear Magnetic Resonance Spectroscopy and X-Ray Crystallography. *Biochemistry* **1992**, *31*, 9609−9621.

(10) Wilson, I. A.; Skehel, J. J.; Wiley, D. C. Structure of the Haemagglutinin Membrane Glycoprotein of Influenza Virus at 3 Å Resolution. *Nature* **1981**, *289*, 366−373.

(11) Connor, R. J.; Kawaoka, Y.; Webster, R. G.; Paulson, J. C. Receptor Specificity in Human, Avian, and Equine H2 and H3 Influenza Virus Isolates. *Virology* **1994**, *205*, 17−23.

(12) Stencel-Baerenwald, J. E.; Reiss, K.; Reiter, D. M.; Stehle, T.; Dermody, T. S. The Sweet Spot: Defining Virus-Sialic Acid Interactions. *Nat. Rev. Microbiol.* **2014**, *12*, 739−749.

(13) Carr, C. M.; Kim, P. S. A Spring-Loaded Mechanism for the Conformational Change of Influenza Hemagglutinin. *Cell* **1993**, *73*, 823−832.

(14) Floyd, D. L.; Ragains, J. R.; Skehel, J. J.; Harrison, S. C.; van Oijen, A. M. Single-Particle Kinetics of Influenza Virus Membrane Fusion. *Proc. Natl. Acad. Sci. U.S.A.* **2008**, *105*, 15382−15387.

(15) Ivanovic, T.; Choi, J. L.; Whelan, S. P.; Van Oijen, A. M.; Harrison, S. C. Influenza-Virus Membrane Fusion by Cooperative Fold-Back of Stochastically Induced Hemagglutinin Intermediates. *Elife* **2013**, *2*, No. e00333.

(16) Thompson, M. P.; Chien, M. P.; Ku, T. H.; Rush, A. M.; Gianneschi, N. C. Smart Lipids for Programmable Nanomaterials. *Nano Lett.* **2010**, *10*, 2690.

(17) Rawle, R. J.; Boxer, S. G.; Kasson, P. M. Disentangling Viral Membrane Fusion from Receptor Binding Using Synthetic DNA-Lipid Conjugates. *Biophys. J.* **2016**, *111*, 123−131.

(18) Liu, K. N.; Boxer, S. G. Target Membrane Cholesterol Modulates Single Influenza Virus Membrane Fusion Efficiency but Not Rate. *Biophys. J.* **2020**, *118*, 2426−2433.

(19) Goronzy, I. N.; Rawle, R. J.; Boxer, S. G.; Kasson, P. M. Cholesterol Enhances Influenza Binding Avidity by Controlling Nanoscale Receptor Clustering. *Chem. Sci.* **2018**, *9*, 2340−2347.

(20) Chan, Y.-H. M.; Lengerich, B. van.; Boxer, S. G. Effects of Linker Sequences on Vesicle Fusion Mediated by Lipid-Anchored DNA Oligonucleotides. *Proc. Natl. Acad. Sci. U.S.A.* **2009**, *106*, 979−984.

(21) Van Lengerich, B.; Rawle, R. J.; Bendix, P. M.; Boxer, S. G. Individual Vesicle Fusion Events Mediated by Lipid-Anchored DNA. *Biophys. J.* **2013**, *105*, 409−419.

(22) Peruzzi, J. A.; Jacobs, M. L.; Vu, T. Q.; Wang, K. S.; Kamat, N. P. Barcoding Biological Reactions with DNA-Functionalized Vesicles. *Angew. Chem.* **2019**, *131*, 18856−18863.
(23) Stengel, G.; Zahn, R.; Höök, F. DNA-Induced Programmable Fusion of Phospholipid Vesicles. *J. Am. Chem. Soc.* **2007**, *129*, 9584−9585.
(24) Liu, K. N.; Boxer, S. G. Single-Virus Content-Mixing Assay Reveals Cholesterol-Enhanced Influenza Membrane Fusion Efficiency. *Biophys. J.* **2021**, *120*, 4832−4841.
(25) Delaveris, C. S.; Webster, E. R.; Banik, S. M.; Boxer, S. G.; Bertozzi, C. R. Membrane-Tethered Mucin-like Polypeptides Sterically Inhibit Binding and Slow Fusion Kinetics of Influenza A Virus. *Proc. Natl. Acad. Sci. U.S.A* **2020**, *117*, 12643−12650.
(26) Block, S.; Zhdanov, V. P.; Höök, F. Quantification of Multivalent Interactions by Tracking Single Biological Nanoparticle Mobility on a Lipid Membrane. *Nano Lett.* **2016**, *16*, 4382−4390.
(27) Chung, M.; Lowe, R. D.; Chan, Y. H. M.; Ganesan, P. V.; Boxer, S. G. DNA-Tethered Membranes Formed by Giant Vesicle Rupture. *J. Struct. Biol.* **2009**, *168*, 190−199.
(28) Ajo-Franklin, C. M.; Yoshina-Ishii, C.; Boxer, S. G. Probing the Structure of Supported Membranes and Tethered Oligonucleotides by Fluorescence Interference Contrast Microscopy. *Langmuir* **2005**, *21*, 4976−4983.
(29) Sauter, N. K.; Wurzburg, B. A.; Hanson, J. E.; Wiley, D. C.; Bednarski, M. D.; Whitesides, G. M.; Skehel, J. J. Hemagglutinins from Two Influenza Virus Variants Bind to Sialic Acid Derivatives with Millimolar Dissociation Constants: A 500-MHz Proton Nuclear Magnetic Resonance Study. *Biochemistry* **1989**, *28*, 8388−8396.
(30) Chan, Y.-H. M.; Lenz, P.; Boxer, S. G. Kinetics of DNA-Mediated Docking Reactions between Vesicles Tethered to Supported Lipid Bilayers. *Proc. Natl. Acad. Sci. U.S.A* **2007**, *104*, 18913−18918.
(31) Li, Y.; Han, X.; Lai, A. L.; Bushweller, J. H.; Cafiso, D. S.; Tamm, L. K. Membrane Structures of the Hemifusion-Inducing Fusion Peptide Mutant G1S and the Fusion-Blocking Mutant G1V of Influenza Virus Hemagglutinin Suggest a Mechanism for Pore Opening in Membrane Fusion. *J. Virol.* **2005**, *79*, 12065−12076.
(32) Lai, A. L.; Park, H.; White, J. M.; Tamm, L. K. Fusion Peptide of Influenza Hemagglutinin Requires a Fixed Angle Boomerang Structure for Activity. *J. Biol. Chem.* **2006**, *281*, 5760−5770.
(33) Lai, A. L.; Tamm, L. K. Shallow Boomerang-Shaped Influenza Hemagglutinin G13A Mutant Structure Promotes Leaky Membrane Fusion. *J. Biol. Chem.* **2010**, *285*, 37467−37475.
(34) Bustamante, C.; Bryant, Z.; Smith, S. B. Ten Years of Tension: Single-Molecule DNA Mechanics. *Nature* **2003**, *421*, 423−427.
(35) Wilhelm, K. B.; Morita, S.; McAffee, D. B.; Kim, S.; O'Dair, M. K.; Groves, J. T. Height, but Not Binding Epitope, Affects the Potency of Synthetic TCR Agonists. *Biophys. J.* **2021**, *120*, 3869−3880.
(36) Ginger, L.; Malsam, J.; Sonnen, A. F. P.; Morado, D.; Scheutzow, A.; Söllner, T. H.; Briggs, J. A. G. Arrangements of Proteins at Reconstituted Synaptic Vesicle Fusion Sites Depend on Membrane Separation. *FEBS Lett.* **2020**, *594*, 3450−3463.
(37) Dietz, J.; Oelkers, M.; Hubrich, R.; Pérez-Lara, A.; Jahn, R.; Steinem, C.; Janshoff, A. Forces, Kinetics, and Fusion Efficiency Altered by the Full-Length Synaptotagmin-1 -PI(4,5)P 2 Interaction in Constrained Geometries. *Nano Lett.* **2021**, DOI: 10.1021/acs.nanolett.1c02491.
(38) Qi, S. Y.; Groves, J. T.; Chakraborty, A. K. Synaptic Pattern Formation during Cellular Recognition. *Proc. Natl. Acad. Sci. U.S.A.* **2001**, *98*, 6548−6553.

Supporting Information

Modulating the influenza A virus – target membrane fusion interface with synthetic DNA-lipid receptors

*Elizabeth R. Webster‡, Katherine N. Liu‡, Robert J. Rawle, and Steven G. Boxer**

Department of Chemistry, Stanford University, Stanford, California 94305, United States

‡ERW and KNL contributed equally.

*Corresponding Author Email: sboxer@stanford.edu

Table S1. DNA-lipid sequences.

Name	DNA sequence (5'-3')
A	Biotin-TTT TTT TTT TTT TTT TTT TTT TTT
A'	Lipid-AAA AAA AAA AAA AAA AAA AAA AAA
B	Lipid-TAG TAT TCA ACA TTT CCG TGT CGA
B'	Lipid-TCG ACA CGG AAA TGT TGA ATA CTA
L24B'	Lipid-CCC CCC CCC CCC CCC CCC CCC CCC TCG ACA CGG AAA TGT TGA ATA CTA
L42B'	Lipid-CCC CCC CCC CCC CCC CCC CCC CCC CCC CCC CCC CCC CCC CCC CCC CCC CCC CCC TCG ACA CGG AAA TGT TGA ATA CTA
L72B'	Lipid-CCC CCC CCC CCC CCC CCC CCC CCC CCC CCC CCC CCC CCC CCC CCC CCC CCC CCC CCC CCC CCC CCC CCC CCC CCC CCC CCC CCC TCG ACA CGG AAA TGT TGA ATA CTA
C	TTG AGA TCT TCC ATA TGC TGA GAG GGA TTG TGT CGA GAT AAG GCT GTG
C'	CAC AGC CTT ATC TCG ACA CAA TCC CTC TCA GCA TAT GGA AGA TCT CAA
D	TTG AGA TCT TCC ATA TGC TGA GAG GGA TTG TGT CGA GAT AAG GCT GTG GTG GTA TTG CGC TAT GAG TAC TAA
D'	TTA GTA CTC ATA GCG CAA TAC CAC CAC AGC CTT ATC TCG ACA CAA TCC CTC TCA GCA TAT GGA AGA TCT CAA
B'L24E'	ACG CCT ATT GTT AAA GTG TGT CCT CCC CCC CCC CCC CCC CCC CCC CCC TCG ACA CGG AAA TGT TGA ATA CTA

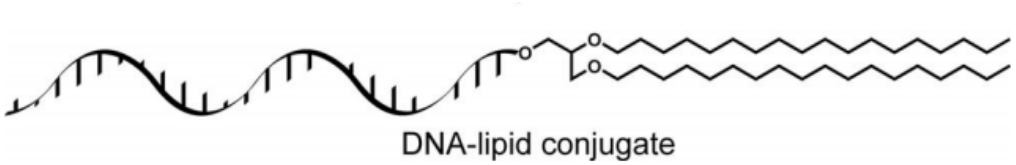

Figure S1. Structure of DNA-lipid conjugates as previously published.[1]

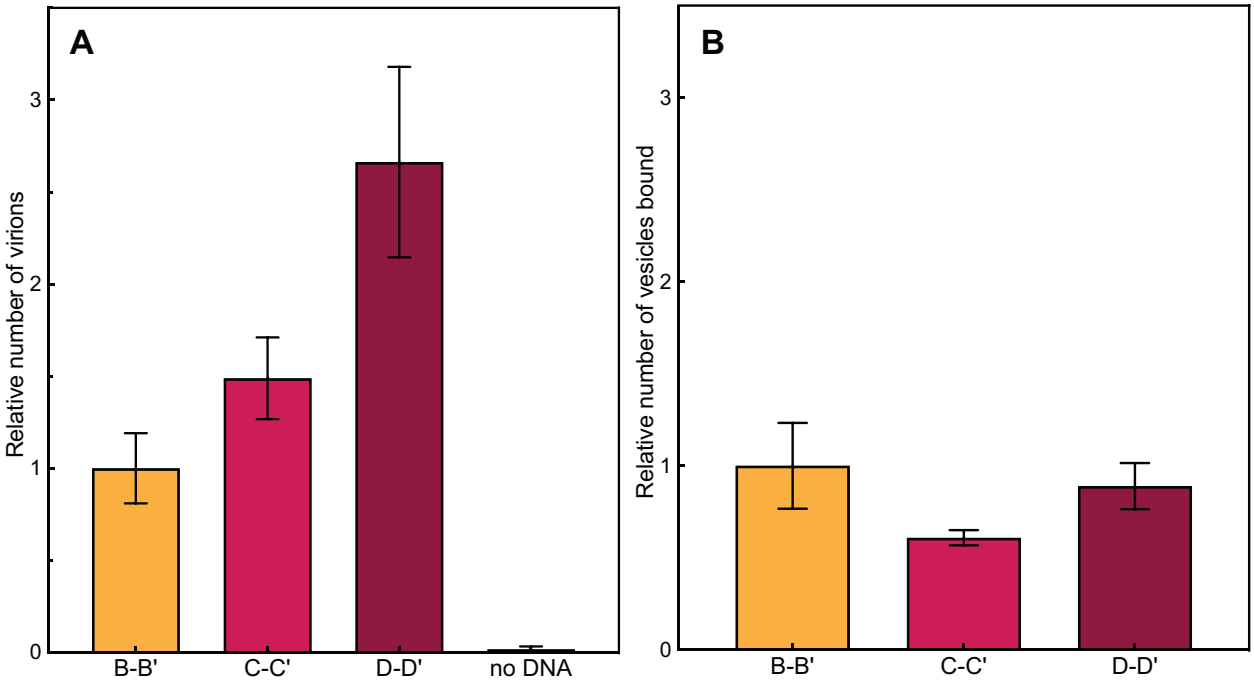

Figure S2. DNA tether length increases the number of IAV that bind to a SLB but has no effect on the extent of vesicle binding.
The DNA sequences that comprise each tether are listed in pairs (bilayer anchored-IAV or vesicle anchored). A) As in Fig. 2A, increasing DNA tether length increases the extent of IAV binding to a supported lipid bilayer (SLB, 69.9 POPC: 20 DOPE: 10 CH: 0.1 OG-DHPE). Values represent the relative number of virions bound per microscope field of view (FOV) ± standard deviation within sample replicates, where the value for B-B′ is normalized to 1. B) In contrast, increasing DNA tether length does not significantly change the number of vesicles (99 POPC: 1 TR-DHPE) that bind to a SLB. Values represent the relative number of vesicles bound per microscope FOV ± standard deviation within sample replicates, where the value for B-B′ is normalized to 1.

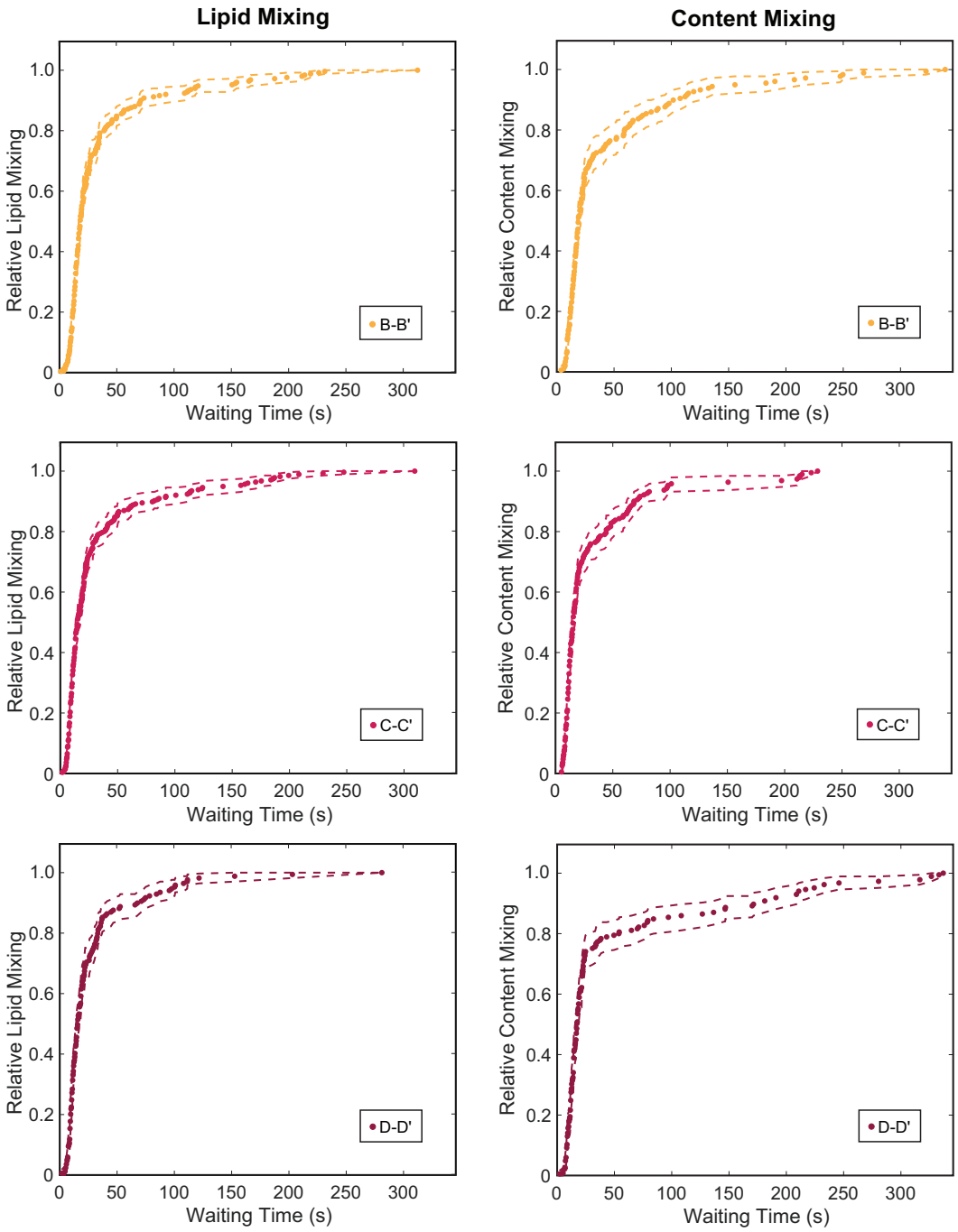

Figure S3. Individual CDFs for IAV lipid and content mixing (merged in Figure 2BC).
As in Figure 2, wait times from pH drop to lipid or content mixing for individual content mixing events are plotted as CDFs. Dashed lines represent bootstrap resampling error (95% confidence intervals). Efficiencies were calculated by dividing the number of vesicles that underwent dequenching by the total number of vesicles bound. Absolute lipid mixing efficiencies: B-B': 250/740 (33%), C-C': 276/705 (39%), D-D': 169/633 (27%). Absolute content mixing efficiencies: B-B': 107/3755 (2.8%), C-C': 191/4851 (3.9%), D-D': 185/9296 (1.9%). Kinetic data for each DNA tether were compiled from at least two different independent viral preparations.

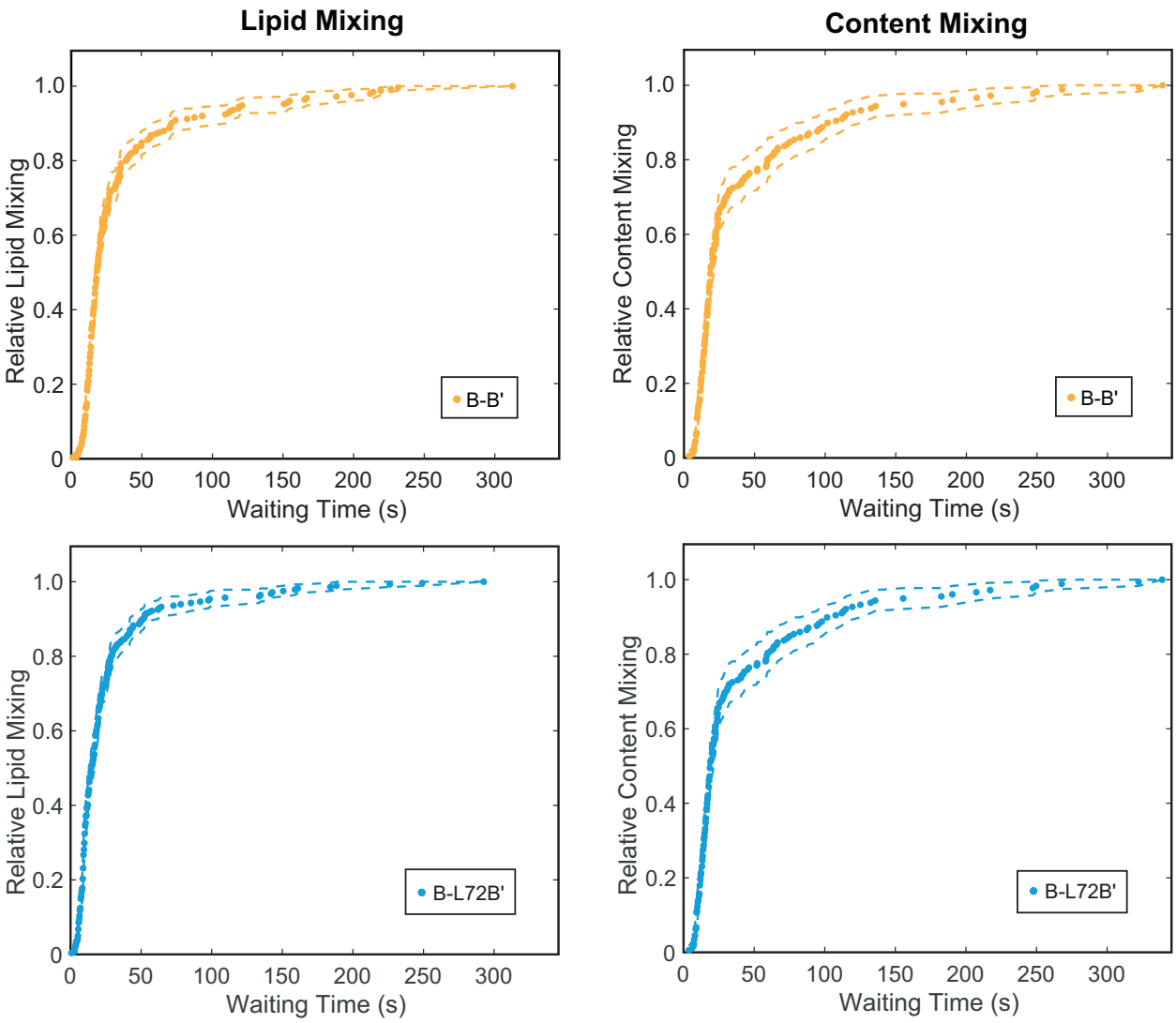

Figure S4. Individual CDFs for IAV lipid and content mixing (merged in Figure 3BC).
As in Figure 3, wait times from pH drop to lipid or content mixing for individual content mixing events are plotted as CDFs. Dashed lines represent bootstrap resampling error (95% confidence intervals). Absolute lipid mixing efficiencies: B-B': 250/740 (34%), B-L72B': 281/776 (36%). Absolute content mixing efficiencies: B-B': 107/3755 (2.8%), B-L72B': 254/4399 (5.8%). Kinetic data for each DNA tether were compiled from at least two different independent viral preparations.

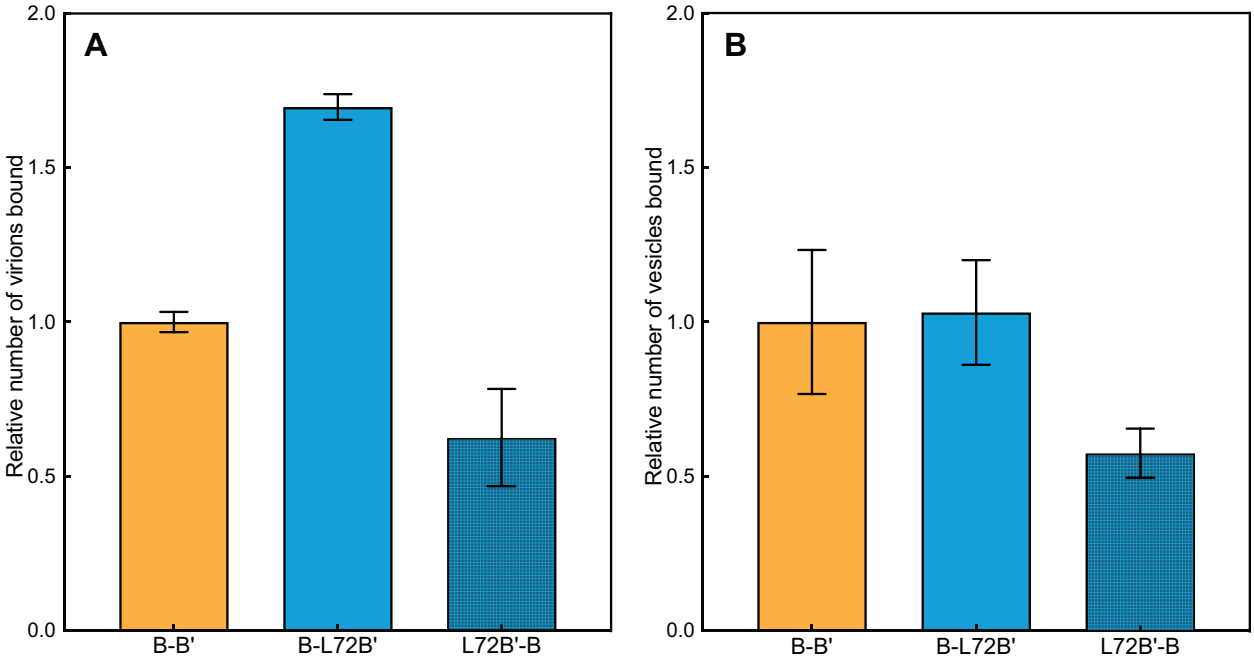

Figure S5. The addition of a flexible linker to DNA tethers only increases viral binding when the linker is IAV-proximal.
The DNA sequences that comprise each tether are listed in pairs (bilayer anchored - IAV or vesicle anchored). A) As in Fig. 3A, adding a linker to the IAV-proximal end of a DNA tether increases the extent of viral binding, while adding a linker to the bilayer-proximal end of a DNA tether decreases IAV binding. Values represent the relative number of virions bound per microscope FOV ± standard deviation within sample replicates, where the value for B-B' is normalized to 1. B) Adding a linker to the vesicle-proximal end of a DNA tether has no effect on vesicle (99 POPC: 1 TR-DHPE) binding. As in IAV binding, adding a linker to the bilayer-proximal end of a DNA tether decreases vesicle binding. Values represent the relative number of vesicles bound per microscope FOV ± standard deviation within sample replicates, where the value for B-B' is normalized to 1.

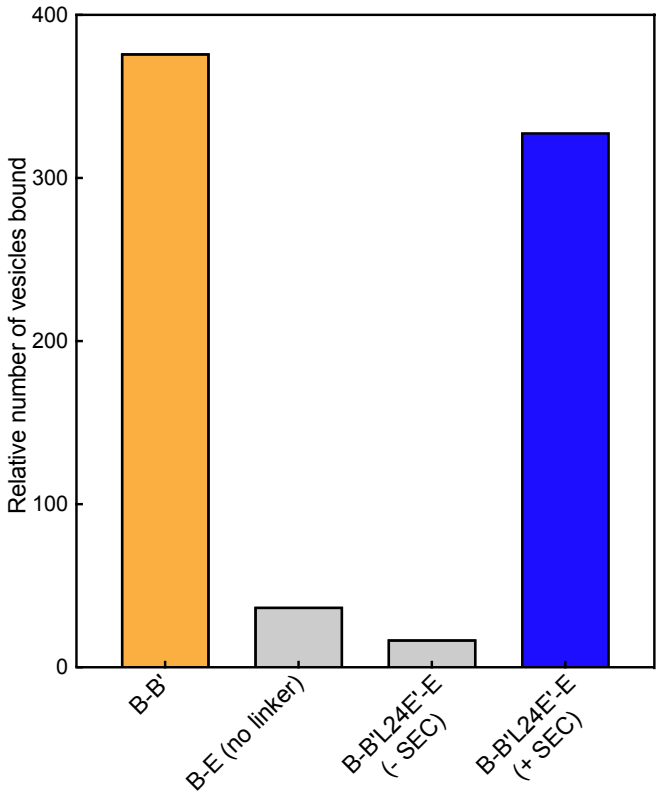

Figure S6. DNA oligo (B'L24E') binds specifically to vesicle-anchored (B) and bilayer-anchored (E) DNA-lipids to form a DNA tether with a flexible hinge. Excess DNA must be filtered away from vesicles (99 POPC: 1 TR-DHPE) on a size exclusion column (SEC) prior to binding, otherwise only minimal binding is observed.

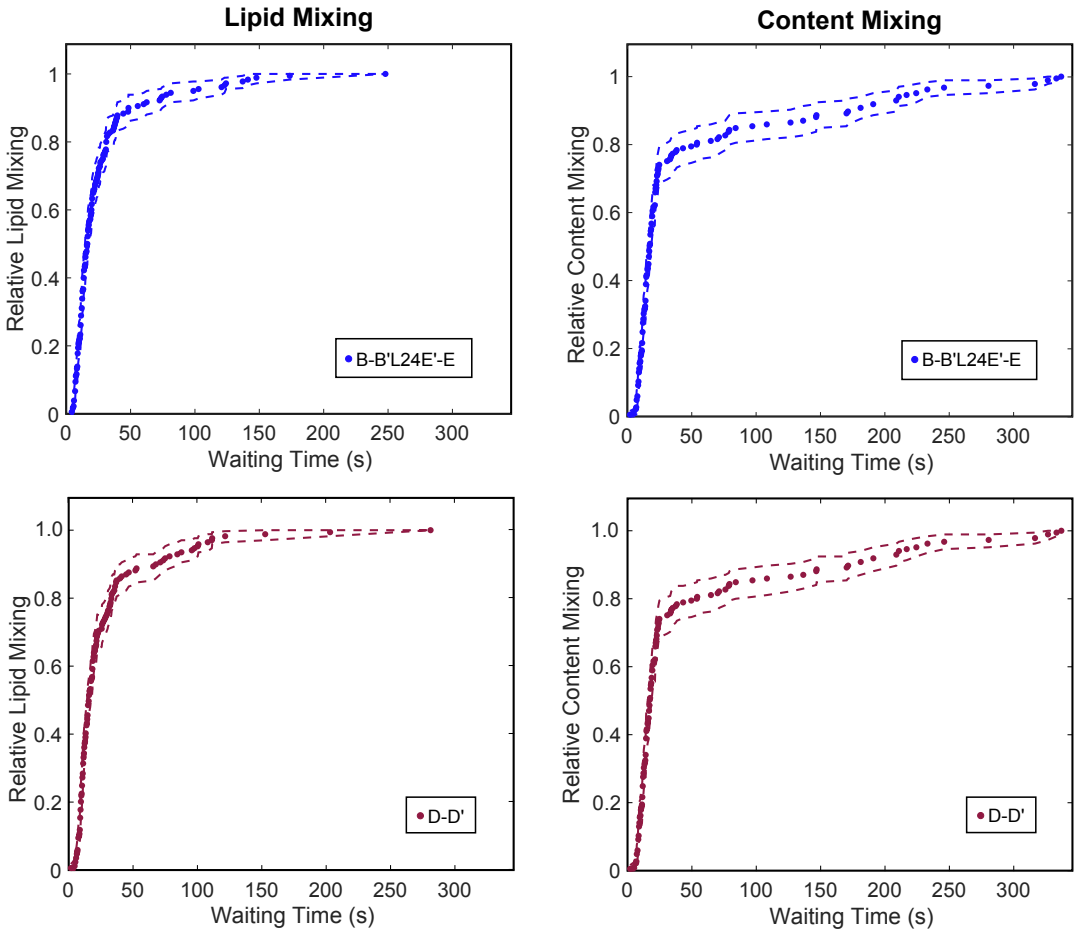

Figure S7. Individual CDFs for IAV lipid and content mixing (merged in Figure 4AB).
As in Figure 4, wait times from pH drop to lipid or content mixing for individual content mixing events are plotted as CDFs. Dashed lines represent bootstrap resampling error (95% confidence intervals). Absolute lipid mixing efficiencies: B-B'L24E'-E: 213/763, D-D': 169/633 (27%). Absolute content mixing efficiencies: B-B'L24E'-E: 98/2542 (3.8%), D-D': 185/9298 (1.9%). Kinetic data for each DNA tether were compiled from at least two different independent viral preparations.

Supporting Movie Information

Movie S1. A representative video micrograph of lipid mixing of Texas-Red labeled vesicles bound to surface-tethered influenza A virions (unlabeled). The frame rate has been sped up 15X to facilitate viewing. The total real time of the movie is 340 sec. The pH of the system is lowered from 7.4 to 5.1 at frame 1.

Movie S2. A representative video micrograph of content mixing of SRB content-labeled vesicles bound to surface-tethered influenza A virions (unlabeled). The frame rate has been sped up 15X to facilitate viewing. The total real time of the movie is 340 sec. The pH of the system is lowered from 7.4 to 5.1 at frame 1.

References

1. Chan, Y.-H. M.; Van Lengerich, B.; Boxer, S. G. Lipid-Anchored DNA Mediates Vesicle Fusion as Observed by Lipid and Content Mixing. *Biointerphases* **2008**, *3* (2)